https://doi.org/10.46813/2025-159-020

UDC 539:1, 42-43,669-1

RADIATION-INDUCED SEGREGATION IN $CrFe_2MnNi$ HIGH-ENTROPY ALLOY AND ITS STRENGTHENED VERSION

G.D. Tolstolutska, O.C. Kalchenko, S.O. Karpov, M.A. Tikhonovsky, B.S. Sungurov
National Science Center "Kharkiv Institute of Physics and Technology", Kharkiv, Ukraine
E-mail: g.d.t@kipt.kharkov.ua

A single-phase FCC high-entropy alloy (HEA) of 20%Cr-40%Fe-20%Mn-20%Ni composition and its oxide-dispersion-strengthened (ODS) version with yttrium and zirconium oxides were irradiated with 20 keV helium ions to a dose of 4.8 dpa (11.7 at.% He) at room temperature. After subsequent annealing at 500…750 °C, transmission electron microscopy (TEM) combined with scanning transmission electron microscopy and energy-dispersive X-ray spectrometry (STEM/EDS) was used to characterize the radiation-induced defects and microstructural changes. Irradiation promoted the formation of a high density of helium bubbles in both alloys, whereas chromium precipitation was observed exclusively in the ODS alloy. The possible mechanisms underlying this precipitation are discussed.

INTRODUCTION

The phenomenon of irradiation-induced segregation caused by neutron irradiation in nuclear structural materials was discovered in 1973 [1]. The results of great deal of research have shown that irradiation can accelerate the diffusion of alloying elements and change their segregation state, thus produce thermodynamically impossible phase transformations, namely, irradiation-induced segregation. Under irradiation, the local concentration gradients make the solute atoms or impurities redistribute, resulting in enrichment or depletion of alloying elements at free surfaces, dislocations, dislocation loops, vacancies, grain boundaries or phase boundaries in alloys.

The irradiation-induced segregation and irradiation-induced phase transformation are important phenomena related to alloy phase stability. They interact with each other, and it is not possible to fully differentiate the two in terms of their effects on material properties. Along with the study and discovery of the organization of the solid solution phase, nanocrystalline and amorphous phases of HEAs, the phase stability of HEAs has become key to the study of their properties and applications under irradiation.

Overall, the Ni and Co elements in most of the HEAs are more likely to aggregate at grain boundaries or near irradiation defects, while Fe, Cr, Mn, and Pd elements are depleted at these sites. Moreover, as the addition of alloying elements of the multi-principal solid solution alloys increases, irradiation-induced segregation near grain boundaries and irradiation defects is significantly inhibited, and the type of alloying element also plays a role in the irradiation-induced segregation behaviour of HEAs. The results from numerous studies have shown that the irradiation-induced elemental segregation at grain boundaries and dislocation loops in HEAs is the same as that of the conventional alloy steels (austenitic stainless steels), which is the result of the unequal exchange rate among solute atoms, interstitial atoms and vacancies [2].

Production of helium and helium embrittlement are ubiquitous in metallic materials as they are used in nuclear energy technology. Microstructural analysis of these irradiated materials shows that when the helium concentration reaches a certain amount, concentrated helium bubbles with nanometer size will form in the matrix, at dislocation, grain boundaries and phase boundaries. The existence of these helium bubbles changes the internal microstructure of the materials, causing local lattice distortions, stress redistribution, swelling, and, in some cases, segregation of elements [3].

Studies on elemental segregation in HEAs are mainly focused on the Cantor alloy FeCrMnNiCo and its subsystems. FeCrMnNiCo is widely considered to be an exemplar high-entropy alloy, which is stable as a single solid-solution phase at all temperatures below its melting point. However, the formation of two distinct types of Cr-rich precipitate in coarse-grained FeCrMnNiCo is reported following prolonged exposures at 700 °C [4]. The precipitates were identified as $M_{23}C_6$ and the σ phase, and their formation in unworked material during heat treatments without an applied stress indicated that they are equilibrium phases. As a result, the previous belief that FeCrMnNiCo is thermodynamically stable as a single solid solution at all temperatures below its solidus can no longer be considered valid.

We investigated the alloy $CrFe_2MnNi$ and showed that after irradiation with 1.4 MeV Ar^+ ions (50 dpa, 4 at.% Ar) at 600 °C only a uniform distribution of elements is observed. However, the irradiation of this alloy with 20 keV helium ions and subsequent annealing at 500 °C causes the formation of the bubbles and precipitates. EDS maps reveal a segregation of only chromium atoms [5].

The aim of this work is to conduct a more extended study of the microstructure evolution of a high-entropy alloy $CrFe_2MnNi$ and it's strengthened with yttrium – zirconium oxides version irradiated at room temperature to a pick dose of 4.8 dpa and a pick helium concentration of 11.7 at.% and subsequently annealed at 500…750 °C.

1. EXPERIMENTAL DETAILS

High entropy alloy with the nominal compositions (in at. %) of 20Cr-40Fe-20Mn-20Ni ($CrFe_2MnNi$) was produced by arc melting in a high-purity argon in a water-cooled copper mould. The purity of alloying elements was above 99.9%. To ensure chemical homogeneity, the ingots were flipped over and re-melted a least 5 times. The alloy was studied after homogenization. Homogenization annealing of ingots was carried out at 1050 °C and lasted for 24 h.

Alloys were subjected to thermomechanical treatment (TMT) that consisted in deformation of the rolling at room temperature from 6 to 0.2 mm with intermediate annealing at 1100 °C for 3 h. Finishing annealing after decreasing sample thickness to 0.2 mm was carried out at 1100 °C for 1 h [6].

The process of mechanical alloying of HEA powders with nanosized yttrium-zirconium oxides was carried out in a high energy ball mill in an inert atmosphere of argon. Powder compaction and mechanical-thermal processing to obtain oxide-strengthened $CrFe_2MnNi$ HEA (ODS HEA) are described in [7].

The samples were implanted with 20 keV He^+ ions to a dose of $1 \cdot 10^{21}$ m^{-2}. Irradiations were performed with irradiation facility in accelerating-measuring system "ESU-2" [8]. Ion stopping distribution for 20 keV helium ions (in at.%) and irradiation damages (in dpa) have been calculated with the software The Stopping and Range of Ions in Matter (SRIM 2008) with a displacement threshold energy of 40 eV [9, 10] (Fig. 1).

The ion flux was $1 \cdot 10^{18}$ He/($m^2 \cdot s$). Ion implantation was carried out at normal ion incidence. The temperature of the sample did not exceed 25 °C during irradiation.

The evolution of microstructure was investigated after post-implantation annealing at 500…750 °C for 10 min. Annealing was used as method for investigation of exposure of the short-term high thermal flux on the materials of advanced reactors. Samples for TEM studies were prepared as disks of 3 mm in diameter. Thin foils were obtained by mechanically thinning of the disks to ~ 130 μm, followed by electropolishing and short-term annealing. Final thinning was performed by jet electropolishing from the back side of the sample using a solution of 5% perchloric acid and 95% ethanol until perforation.

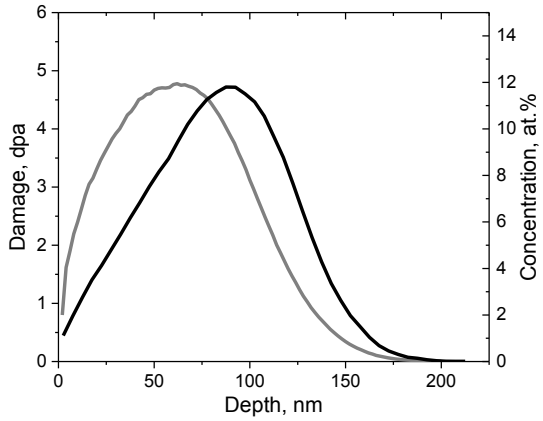

Fig. 1. Calculated profiles of damages and concentrations of 20 keV He^+ ions in 20Cr-40Fe-20Mn-20Ni alloy irradiated to a dose of $1 \cdot 10^{21}$ m^{-2}

The microstructure of the alloys was studied by electron microscope JEM-2100. Energy dispersive X-ray spectrometry was used to characterize the radiation defects and microstructural changes.

2. RESULTS AND DISCUSSION

According to X-ray analysis, the typical microstructure of a $CrFe_2MnNi$ high-entropy alloy and matrix of ODS HEA are single-phase with FCC crystal lattice [7]. The average grain size of HEA and ODS HEA were estimated to be 3.47 and 1.61 μm, respectively. The initial dislocation density in all studied alloys was varied from $1.7 \cdot 10^{12}$ to $2.5 \cdot 10^{12}$ m^{-2} [7].

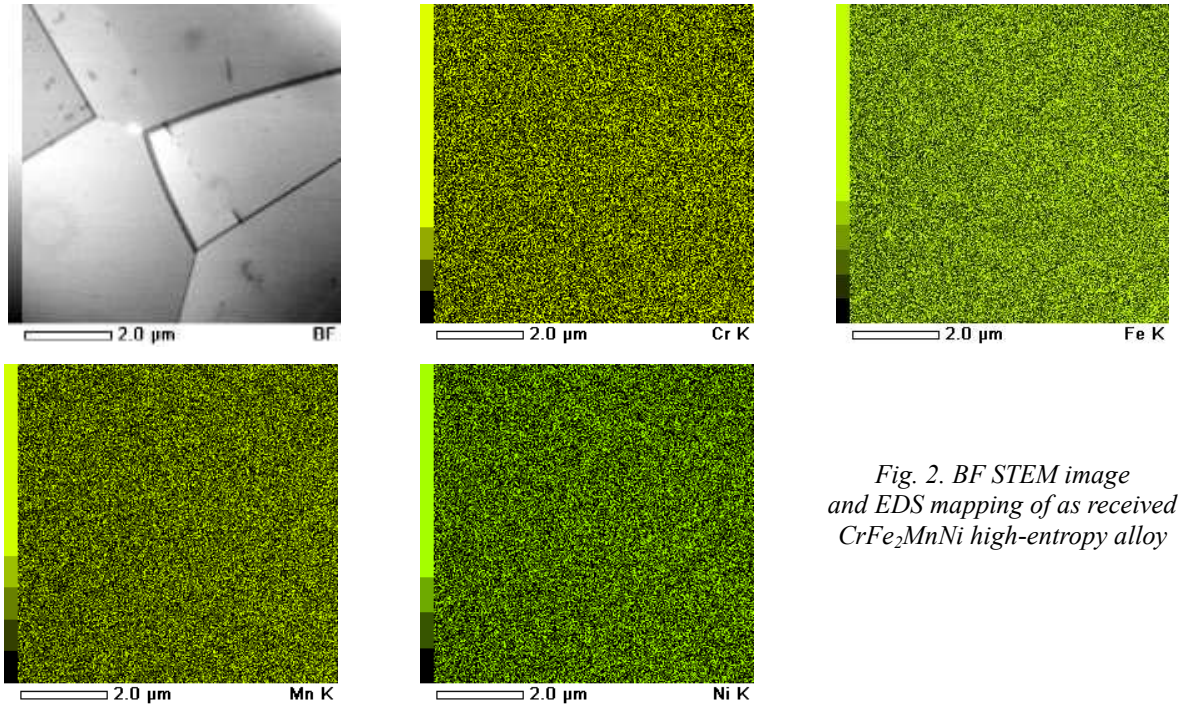

Fig. 2. BF STEM image and EDS mapping of as received $CrFe_2MnNi$ high-entropy alloy

Fig. 2 shows the bright-field STEM image and EDS mapping of as received $CrFe_2MnNi$ high-entropy alloy. It is clearly visible that there are no precipitates in the matrix.

Fig. 3 shows the bright-field STEM image of precipitates and EDS mapping of ODS $CrFe_2MnNi$ high-entropy alloy. It is clearly visible that there are two kinds of precipitates in the matrix according to the chemical composition.

The larger ones marked by arrows are the Cr-Mn-O rich precipitates. Smaller precipitates contain elements of Y and Zr. The compositional analysis performed by means of energy dispersive spectroscopy has indicated that these precipitates are $(Y,Zr)_xO_y$.

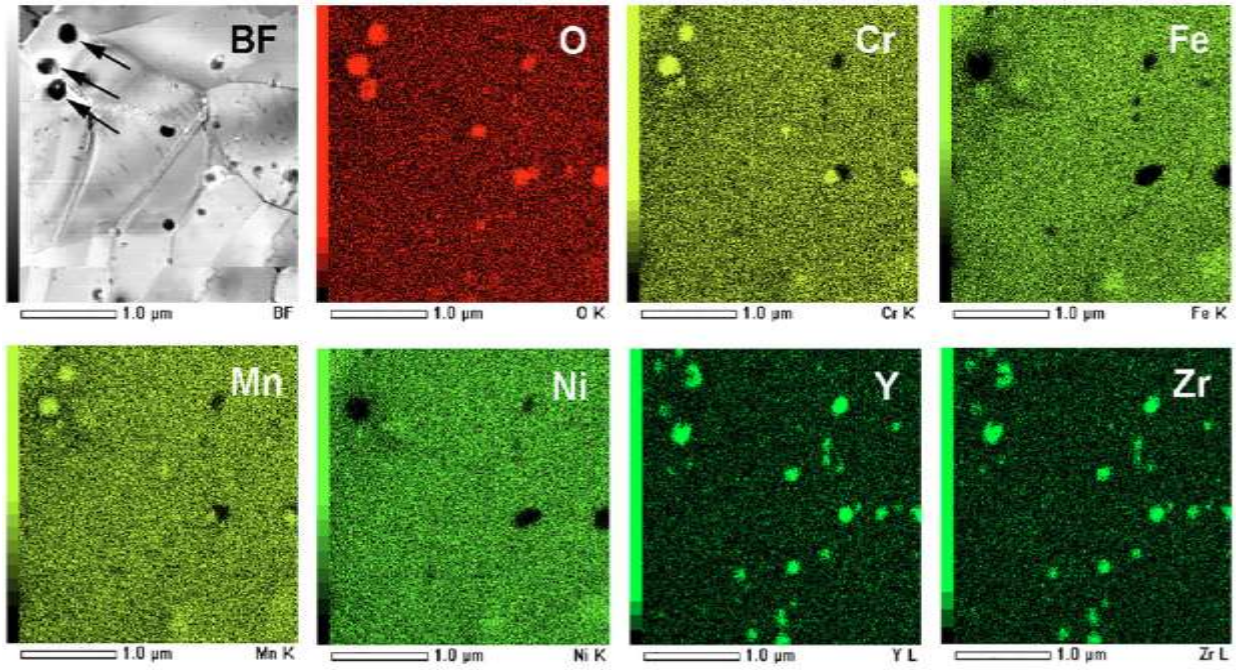

Fig. 3. BF STEM image and EDS mapping of as received ODS – $CrFe_2MnNi$ high-entropy alloy

Irradiation of the $CrFe_2MnNi$ alloy and its ODS counterpart containing yttrium and zirconium oxides, followed by thermal annealing, results in the formation of helium bubbles in both materials (Fig. 4). After annealing at 500 °C, the bubbles that develop in the ODS alloy reach an average size of about 2 nm (see Fig. 4,a). For comparison, earlier investigations of the reference $CrFe_2MnNi$ alloy under similar conditions demonstrated the appearance of noticeably finer bubbles, with an average diameter of only ~ 1.1 nm [5].

When the annealing temperature is further increased to 750 °C, the bubbles in the ODS alloy undergo pronounced coarsening, attaining a size of nearly 50 nm (see Fig. 4,b). Under the same thermal treatment, however, the alloy without oxide dispersion exhibits considerably smaller bubbles, which on average do not exceed 25 nm in diameter (see Fig. 4,c).

It should be noted that the present study was not intended to provide a detailed analysis of helium porosity. Instead, the study was primarily directed toward elucidating the evolution of chromium segregation processes accompanying the formation of helium bubbles. Within this framework, Fig. 4 should be regarded as an illustrative representation, providing qualitative insight into the dependence of bubble size and density on annealing temperature and alloy composition.

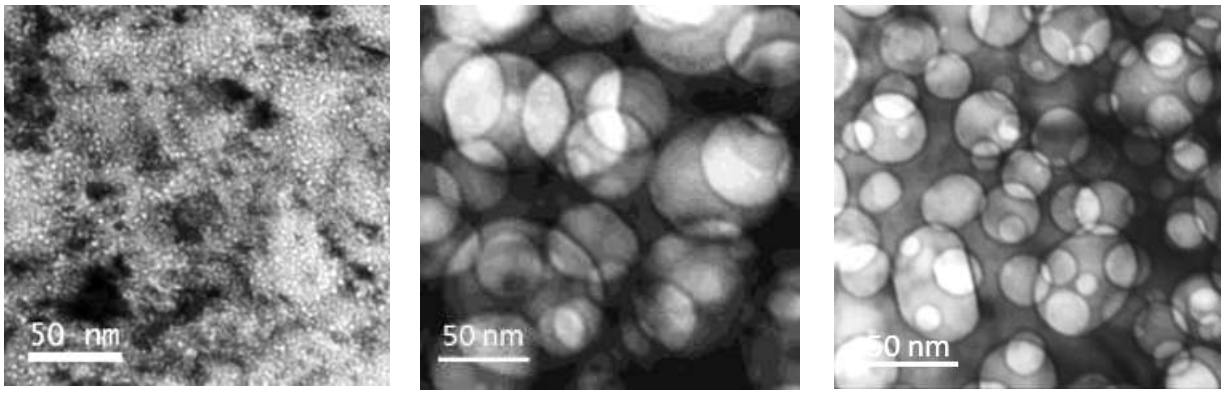

a *b* *c*

Fig. 4. TEM micrographs of alloys irradiated with 20 keV He^+ ions to a dose of $1 \cdot 10^{21}$ m^{-2} at T_{room} and annealed at 500 (a) and 750 °C (b, c) during 10 min for ODS $CrFe_2MnNi$ (a, b) and $CrFe_2MnNi$ HEA (c)

Fig. 5 shows the bright-field image under STEM mode and the chemical analysis for Fe, Cr, Mn, Ni for $CrFe_2MnNi$ alloy irradiated and annealed during 10 min at 750 °C. It is clearly shown that Fe, Cr, Mn, Ni were almost homogeneously distributed in the irradiated alloys and no precipitates were found in this material.

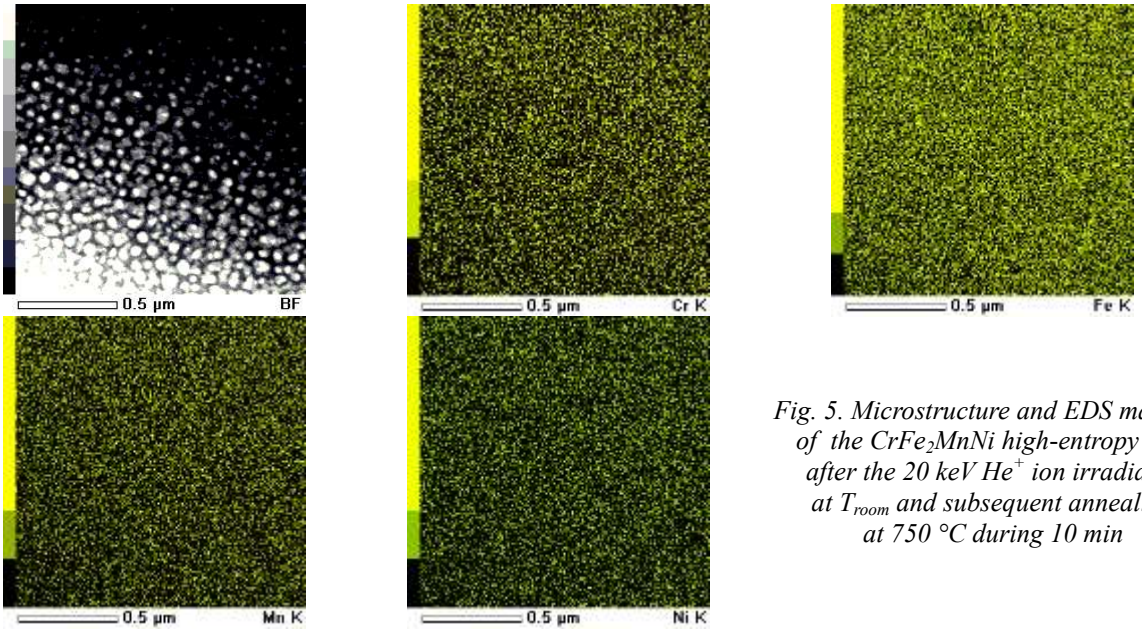

Fig. 5. Microstructure and EDS mapping of the $CrFe_2MnNi$ high-entropy alloy after the 20 keV He^+ ion irradiation at T_{room} and subsequent annealing at 750 °C during 10 min

Fig. 6 shows the bright-field image under STEM mode and the chemical analysis for Fe, Cr, Mn, Ni, and oxides for irradiated and annealed ODS $CrFe_2MnNi$ alloy. It is shown that Fe, Mn, Ni were almost homogeneously distributed in the irradiated alloys. On the other hand, Cr are enriched in the matrix. Thin Film Standardless Quantitative Analysis from X-ray energy dispersive spectroscopy of matrix in $CrFe_2MnNi$ alloy and of an area with chromium segregation in ODS $CrFe_2MnNi$ alloy after irradiation and subsequently annealed at 750 °C confirm this observation (Fig. 7).

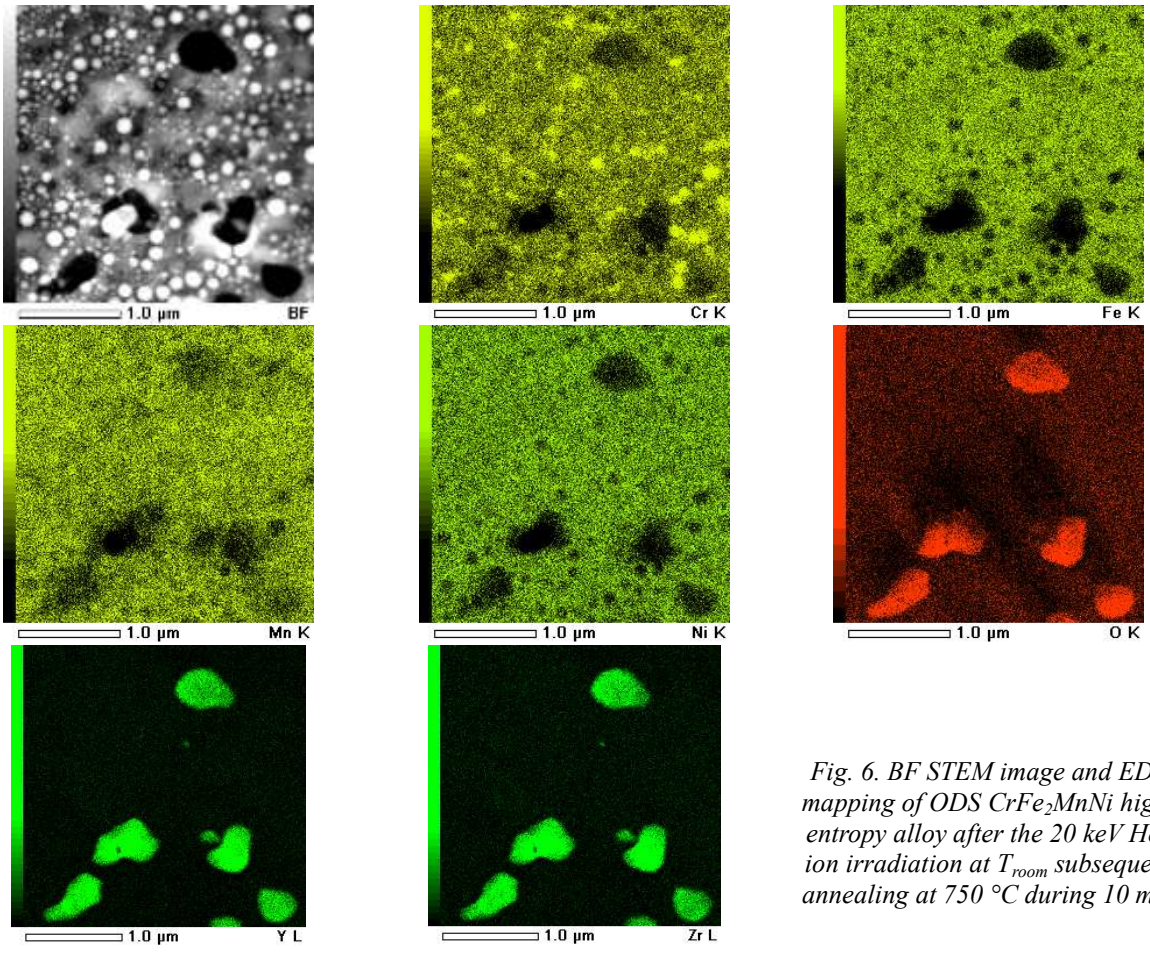

Fig. 6. BF STEM image and EDS mapping of ODS $CrFe_2MnNi$ high-entropy alloy after the 20 keV He^+ ion irradiation at T_{room} subsequent annealing at 750 °C during 10 min

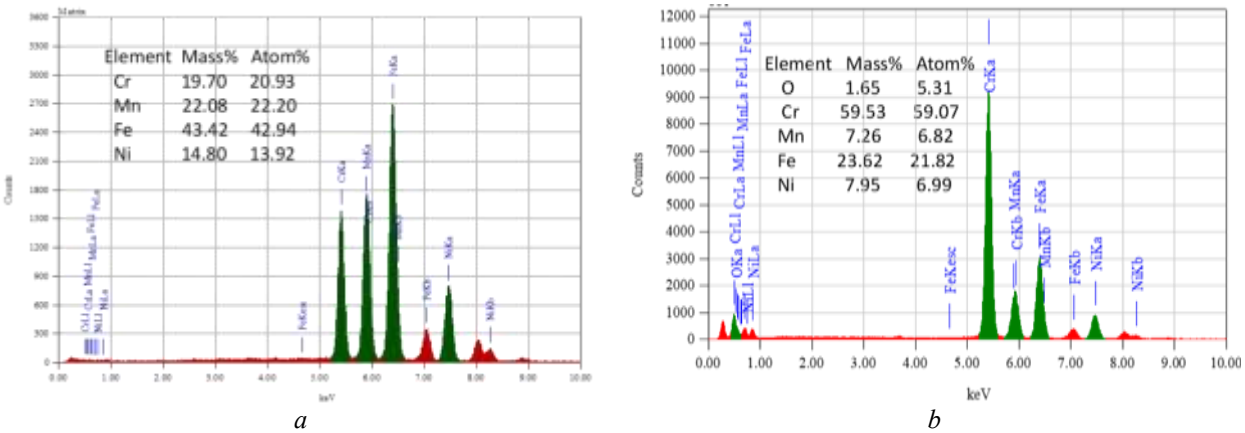

a *b*

Fig. 7. X-ray energy dispersive spectra of ODS $CrFe_2MnNi$ high-entropy alloys after irradiation and subsequent annealing at 750 °C for the matrix (a) and segregation (b)

The spectrum from the matrix shows the ratio of elements close to the nominal one. The spectrum from the precipitate shows enrichment in chromium up to 59 at.%

It should be noted that annealing at 750 °C for 10 min of the as-received ODS $CrFe_2MnNi$ alloy does not lead to obvious segregation of chromium (Fig. 8).

But the formation of two distinct types of Cr-rich precipitate in the Co containing coarse-grained FeCrMnNiCo alloy is reported following prolonged exposures at 700 °C [4]. The precipitates were identified as $M_{23}C_6$ and the σ phase, and their formation during heat treatments without an applied stress indicated that they are equilibrium phases.

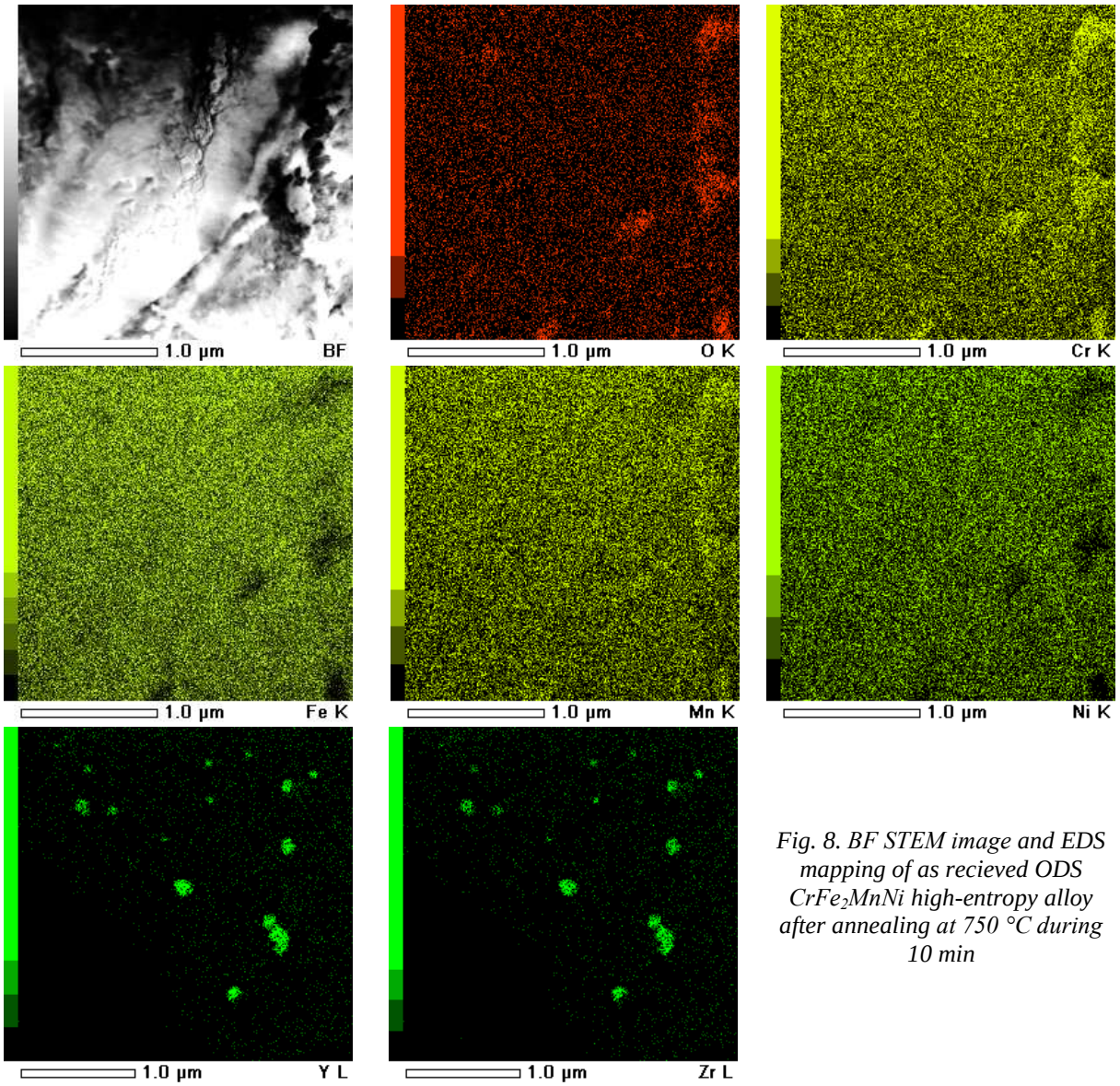

Fig. 8. BF STEM image and EDS mapping of as recieved ODS $CrFe_2MnNi$ high-entropy alloy after annealing at 750 °C during 10 min

As illustrated in Fig. 6, the irradiated samples exhibit isolated bubbles and Cr precipitates, with no discernible regular spatial arrangement of chromium around the helium bubbles. This observation suggests that the formation of bubbles and second-phase precipitates occurs independently, with nucleation events proceeding separately. Their subsequent growth appears to be influenced predominantly by irradiation and subsequent annealing processes. Concurrently, the potential impact of helium on the progression of segregation processes cannot be disregarded.

Helium atoms injected into materials during irradiation combine with vacancies and, consequently, nucleate as bubbles [11]. As the irradiation proceeds, the arrival of more vacancies increases the nuclei in size thereby forming bubbles that act as sinks for both irradiation-produced vacancies and self-interstitials. Such a flow of vacancies and interstitials into the bubbles is accompanied by the preferential flux of each of the elements in the alloy – either towards or away from the bubbles producing the radiation induced segregation (RIS). In this process, the diffusivities of the elements either via vacancies or interstitial atoms play a critical role in the evolution of RIS [12]

Until recently, it was considered reliably established that under irradiation among all five elements (for CrMnFeCoNi HEA) Ni and Co becomes enriched while Fe, Cr, and Mn become depleted in accordance with the Inverse Kirkendall effect (IKE). IKE describes a situation where a vacancy flux, often created by external forces like irradiation, causes a segregation of atoms in a binary alloy. In particular, Mn has an obvious larger and wider depletion profile than Fe and Cr. This trend is consistent with segregation measurements near dislocation loops in Mn-HEAs, and can be rationalized by differences in atomic size between these elements [13].

The atomic size of an element within a solid solution can be quantitatively characterized by the volume size-factor (VSF), which is defined as the fractional change in the average atomic volume per 1 atomic percent increase in the element's concentration within the solid solution [13, 14]. The ranking of VSF values follows the order: Mn > Fe > approximately Cr > Ni > approximately Co. Given that vacancies tend to preferentially exchange positions with atoms of larger atomic radii [15], it is plausible that vacancy migration occurs most rapidly via the largest atoms, such as Mn, thereby accounting for the substantial depletion of Mn observed, with a slightly lesser depletion observed for Cr [16].

The general segregation trend for the single phase-concentrated solid solution alloys (SP-CSAs) is the same – Cr and Fe deplete around the voids. This observed behavior agrees with predictions from density functional theory calculations, which show that vacancy migration energy barriers are lower when moving through Cr and Fe lattice sites compared to Ni and other elements within the SP-CSAs [17].

In our study of the non-Co containing ODS alloy with the composition $CrFe_2MnNi$, Cr segregation was predominantly observed within the matrix phase.

Pronounced Cr enrichment and Co/Ni/Fe depletion was established during the study of segregation phenomena around extended defects including dislocations, stacking faults, and grain boundaries in CoNiCrFe HEAs with different Fe concentrations [18]. The driving force for segregation usually competes with chemical short-range ordering formation. Based on the comparative analysis of segregation energies derived from various methods, it was demonstrated that segregation entropy is a crucial factor influencing segregation behavior in HEAs and must not be overlooked. Relying solely on the enthalpic component is insufficient to fully explain the observed segregation trends [18].

To explain the enrichment of chromium in addition to the IKE mechanism, it is advisable to consider the mechanism of Interstitial Binding (IB). IB considers the phenomenon of a preferential interstitial flux of Cr towards the bubbles via an interstitial binding mechanism [19]. A higher binding energy for Ni-Cr interstitials over Ni-Ni interstitials and the highest diffusivity of Cr via interstitials estimated from recent ab initio calculations supports a Cr dominance in interstitial flux [20].

Two factors that may influence the predictions of the interstitial binding model for Fe-Ni-Cr alloys are the binding energies and migration energies of the interstitials. Simulation results showed that Cr diffuses approximately ten times faster than Fe and Ni via interstitial mechanisms, primarily because Cr has a lower migration energy [20]. These defect energetics calculations suggest that Cr predominantly contributes to the interstitial flux toward sinks during irradiation. This behavior would lead to a Cr enrichment at sink sites [21].

In the present study, beyond the aforementioned mechanisms, defects generated during irradiation with He^+ ions can substantially enhance diffusion processes and induce the decomposition of the solid solution within the examined alloys. These alloys are presumed to be in a nonequilibrium state at the temperature of 750 °C. Furthermore, variations in the formation and evolution of helium-induced porosity between $CrFe_2MnNi$ and ODS CrF_2MnNi alloys (refer to Fig. 4) may influence the characteristics of chromium segregation.

Further research is needed to identify the mechanism of chromium segregation in the matrix during helium ion irradiation and subsequent annealing.

CONCLUSIONS

The phenomenon of chromium (Cr) segregation induced by radiation in the high-entropy alloy $CrFe_2MnNi$ and its strengthened with yttrium and zirconium oxides version has been investigated. The study involved subjecting the alloy to irradiation with 20 keV helium ions at ambient temperature, achieving a dose of 4.8 dpa and a helium concentration of 11.7 at.%. Following irradiation, the samples were subjected to annealing treatments at temperatures ranging from 500 to 750 °C for 10 min to evaluate the effects on Cr segregation and alloy stability.

The formation of helium bubbles was identified following the irradiation of the alloys with helium ions, accompanied by subsequent annealing procedures. The observed bubble diameters averaged approximately 25 nm in the $CrFe_2MnNi$ alloy and 50 nm in the oxide dispersion-strengthened variant.

Annealing at 750 °C for 10 min applied both to the as-received unirradiated $CrFe_2MnNi$ alloy and ODS version did not induce chromium segregation.

Chromium segregation was exclusively detected in the ODS $CrFe_2MnNi$ alloy after irradiation and annealing at 750 °C.

ACKNOWLEDGEMENTS

This work was financially supported by the National Academy of Science of Ukraine (program "Fundamental scientific research on the most important problems of the development of scientific and technical, socio-economic, socio-political, human potential to ensure Ukraine's competitiveness in the world and sustainable development of society and the state").

REFERENCES

1. F.V. Nolfi. *Phase Transformations During Irradiation.* Applied Science. Publishers, 1983.
2. Z. Cheng, J. Sun, X. Gao, et al. Irradiation effects in high-entropy alloys and their applications // *J. of Alloys and Compounds*. 2023, v. 930, p. 166768.
3. H. Chang, S.J. Zinkle, G.S. Was. Materials challenges in nuclear energy // *Acta Mater*. 2013, v. 61, p. 735-758.
4. E.J. Pickering, R. Muñoz-Moreno, H.J. Stone, N.G. Jones. Precipitation in the equiatomic high-entropy alloy CrMnFeCoNi // *Scripta Materialia*. 2016, v. 113, p. 106-109.
5. I.V. Kolodiy, O.S. Kalchenko, M.A. Tikhonovsky, G.D. Tolstolutska. Effect of inert gas ions irradiation on radiation damage of high-entropy alloy $CrFe_2MnNi$ and 18Cr10NiTi steel // *PAST*. 2025, N 2(156), p. 3-11.
6. M.A. Tikhonovsky, A.S. Tortika, I.V. Kolodiy, et al. Microstructure and properties of high enthropy alloys $CoCrFeMnNiV_{0,25}C_{0,175}$ and $CrFe_2MnNiV_{0,25}C_{0,175}$ // *PAST*. 2016, N4(104), p. 37-41.
7. I.V. Kolodiy, O.M. Velikodnyi, M.A. Tikhonovsky, et al. Microstructure and mechanical properties of oxide dispersion strengthened high-entropy alloys CoCrFeMnNi and $CrFe_2MnNi$ // *PAST*. 2021, N 2(132), p. 87-94.
8. G.D. Tolstolutskaya, V.V. Ruzhytskiy, I.E. Kopanetz, et al. Accelerating complex for study of helium and hydrogen behavior in conditions of radiation defects generation // *PAST*. 2010, N 4(65), p. 135-140.
9. SRIM (2008), http://www.srim.org/
10. ASTM E521-96 (2009), ASTM.
11. L.K. Mansur, W.A. Coghlan. Mechanisms of helium interaction with radiation effects in metals and alloys: a review // *J. Nucl. Mater*. 1983, v. 119 (1), p. 1-25.
12. B. Kombaiah, P.D. Edmondson, Y. Wang, L.A. Boatner, Y. Zhang. Mechanisms of radiation-induced segregation around He bubbles in a Fe-Cr-Ni crystal // *J. Nucl. Mater*. 2019, v. 514, p. 139-147.
13. W.Y. Chen, J.D. Poplawsky, Y. Chen, W. Guo, J.W. Yeh. Irradiation-induced segregation at dislocation loops in CoCrFeMnNi high entropy alloy // *Materialia*. 2020, v. 14, p. 100951.
14. H.W. King. Quantitative size-factors for metallic solid solutions // *J. Mater. Sci*. 1966, v. 1, p. 79-90.
15. P.R. Okamoto, L.E. Rehn. Radiation-induced segregation in binary and ternary alloys // *J. Nucl. Mater*. 1979, v. 83, p. 2-23.
16. Xing Wang, Ke Jin, Chun Yin Wong, et al. Understanding effects of chemical complexity on helium bubble formation in Ni-based concentrated solid solution alloys based on elemental segregation measurements // *J. Nucl. Mater.* 2022, v. 569, p. 153902.
17. Xing Wang, Constantinos Hatzoglou, Brian Sneed, et al. Interpreting nanovoids in atom probe tomography data for accurate local compositional measurements // *Nature Communications*. 2020, v. 11, p. 1022.
18. Shihua Ma, Weihong Liu, Qian Li, et al. Mechanism of elemental segregation around extended defects in high-entropy alloys and its effect on mechanical properties // *Acta Materialia*. 2024, v. 264, p. 119537.
19. N.Q. Lam, A.S. Kumar, H. Wiedersich. Kinetics of radiation-induced segregation in ternary alloys / H.R. Brager, J.S. Perrin (Eds.). *Effects of Radiation on Materials*: Eleventh Conference, ASTM STP 782, American Society for Testing of Materials Scottsdale, Arizona, 1982, p. 985-1007.
20. J.D. Tucker, R. Najafabadi, T.R. Allen, D. Morgan. Ab initio-based diffusion theory and tracer diffusion in Ni-Cr and Ni-Fe alloys // *J. Nucl. Mater*. 2010, v. 405 (3), p. 216-234.
21. J.D. Tucker, R. Najafabadi, T.R. Allen, D. Morgan. Determination of solute interstitial interactions in Ni-Cr by first principles // *International Conference on Mathematics* "*Computational Methods & Reactor Physics".* American Nuclear Society, New York, 2009.

Article received 22.09.2025

РАДІАЦІЙНО-ІНДУКОВАНА СЕГРЕГАЦІЯ У ВИСОКОЕНТРОПІЙНОМУ СПЛАВІ $CrFe_2MnNi$ ТА ЙОГО ЗМІЦНЕНІЙ ВЕРСІЇ

Г.Д. Толстолуцька, О.С. Кальченко, С.О. Карпов, М.А. Тихоновський, Б.С. Сунгуров

Однофазний ГЦК високоентропійний сплав (ВЕС) складу 20%Cr-40%Fe-20%Mn-20%Ni та його версія, яка зміцнена оксидами ітрію та цирконію (ДЗО), були опромінені іонами гелію з енергією 20 кеВ до дози 4,8 зна (11,7 ат.% He) за кімнатної температури. Після подальшого відпалу при 500…750 °C для характеристики радіаційно-індукованих дефектів і мікроструктурних змін застосовували просвічувальну електронну мікроскопію (ПЕМ) у поєднанні зі скануючою просвічувальною електронною мікроскопією та енергодисперсійною рентгенівською спектрометрією (СПЕМ/ЕРС). Опромінення зумовило утворення високої щільності гелієвих бульбашок в обох сплавах, тоді як осадження хрому спостерігалося виключно у ДЗО-сплаві. Обговорюються можливі механізми осадження хрому.